Crack closure in friction stir weldment using non-linear model for fatigue crack propagation

Marcello Antonio Lepore[1] | **Angelo Rosario Maligno**[2] | **Filippo Berto**[3]

[1]Department of Industrial Engineering, University of Salerno, Via G. Paolo II 132, 84084 Fisciano, SA, Italy

[2]Institute for Innovation in Sustainable Engineering, University of Derby, Derby, UK

[3]Department of Mechanical and Industrial Engineering, NTNU, Richard Birkelands vei 2b, 7491 Trondheim, Norway

Correspondence
Marcello Antonio Lepore, Department of Industrial Engineering, University of Salerno, Via G. Paolo II 132, 84084. Fisciano, SA, Italy.
Email: malepore@unisa.it

Abstract

The fatigue crack propagation in a friction stir-welded sample has been simulated herein by means of two 3-dimensional finite element method (FEM)-based analyses. Numerical simulations of the fatigue crack propagation have been carried out by assuming a residual stress field as a starting condition. Two initial cracks, observed in the real specimen, have been assessed experimentally by performing fatigue tests on the welded sample. Hence, the same cracks have been placed in the corresponding FE model, and then a remote load with boundary conditions has been applied on the welded specimen. The material behaviour of the welded joint has been modelled by means of the Ramberg-Osgood equation, while the non-linear Kujawski-Ellyin (KE) model has been adopted for the fatigue crack propagation under small-scale yielding (SSY) conditions. Owing to the compressive nature of the residual stress field that acts on a part of the cracked regions, the crack closure phenomenon has also been considered. Then, the original version of the KE law has been modified to fully include the closure effect in the analysis. Later, the crack closure effect has also been assessed in the simulation of fatigue propagation of three cracks. Finally, an investigation of the fracture process zone (FPZ) extension as well as the cyclic plastic zone (CPZ) and monotonic plastic zone (MPZ) extensions have been assessed.

KEYWORDS

crack closure, fatigue crack growth, FSW, Kujawski-Ellyin model, SSY

Nomenclature: A_1, A_2, surface breakthrough points; B_1, B_2, surface breakthrough points; b, fatigue strength exponent; C_1, C_2, middle position breakthrough point; c, fatigue ductility exponent; CCFT, constrained crack faces technique; CPZ, cyclic plastic zone; DBEM, dual boundary element method; E, Young modulus; ERR, energy release rate; FCG, fatigue crack growth; f_{conv}, conversion factor; FEM, finite element method; FPZ, fracture process zone; FSW, friction stir welding; KE, Kujawski-Ellyin model; K_{max}, maximum value of stress intensity factor; $K_{max,tot}$, total value of K_{max}; LCF, low-cycle fatigue; LEFM, linear elastic fracture mechanics; MPZ, monotonic plastic zone; n, strain hardening exponent; n', cyclic hardening exponent; PICC, plasticity-induced crack closure; R, stress ratio; R_s, stress ratio–dependent regions I, II, and III; r_c, radius of cyclic plastic zone; r_m, radius of monotonic plastic zone; SIF, stress intensity factor; SSY, small-scale yielding; U_{cl}, closure factor; VCE, virtual crack extension; x, distance from the crack tip; $\bar{x}$, reduction in area; β, Coffin-Manson exponent; δ^*, length of fracture process zone; υ, Poisson ratio; ρ^*, length of crack extension; ρ_c, crack blunting radius; σ_{max}, maximum cyclic stress; σ_m, local mean stress; σ'_y, fatigue strength coefficient; σ_0, yield strength; σ_u, ultimate strength; σ^c_{max}, maximum cyclic stress component within the CPZ; σ^m_{max}, maximum cyclic stress component within the MPZ; ε^c_{max}, maximum cyclic strain component within the CPZ; ε^m_{max}, maximum cyclic strain component within the MPZ; ϵ'_f, fatigue ductility coefficient; ΔK, stress intensity factor range; ΔK_{appl}, current value of ΔK; ΔK_{eff}, effective value of ΔK; ΔK_{th}, threshold value of ΔK; $\Delta K_{th,eff}$, effective threshold value; $\Delta K_{max,th}$, maximum value of ΔK_{th}; ΔK_{tot}, total stress intensity factor range; $\Delta\sqrt{J}$, energy release rate factor range

1 | INTRODUCTION

In fatigue crack propagation, the material behaviour is generally a function of several conditions such as the load level, load history, stress ratio, stress and strain amplitudes, environment, mixed-mode loading, and small-scale or large-scale yielding. For ductile materials, coalescence of micro-voids, plastic blunting, and re-sharpening of the crack tip are the main causes of crack extension per cycle[1].

Residual stresses substantially change the stress–strain fields in the cracked region and can also induce fractures in the contact surfaces during cyclic loading, which is similar to the other contact mechanisms[1-5]. Ritchie and Suresh have classified these contact mechanisms in which the deformation at the crack tip decreases as zone and contact shielding mechanisms[6,7]. The contact shielding mechanism can be defined as a load transfer between the crack faces, a load transfer that reduces the cyclic deformation at the crack tip per load cycle[6].

Elber[8,9] was the first to discover plasticity-induced crack closure (PICC) by observing that the contact between the crack faces takes place during the cyclic tensile loading, which produces plastic deformations on the crack flank, namely, the plastic wake. In the following years, several other mechanisms of premature contact between the crack faces were proposed: roughness-induced crack closures, oxide-induced crack closures, and phase transformation-induced crack closures. Nowadays, even though many researchers have remarked on the importance of crack closure, some papers have doubted this concept[10-12].

In the last four decades, several models for non-linear fatigue crack propagation have been proposed by researchers in attempts to analytically reproduce the experimental behaviour of cracked samples. In their studies, these researchers have used a range of methods from a simple tensile loaded plate to more complex structural components under both uniaxial and mixed-mode loading conditions. Huffman[13], Shi et al,[14] Kujawski and Ellyin[15,16], Li et al,[17] Noroozi et al,[18] Song et al,[19] Tong et al,[20] and Akhtar et al[21] are some of the researchers who have studied the fatigue behaviour of cracked components under uniaxial or multiaxial non-linear loading conditions. In some cases, the effect of the mean stress on the fatigue crack behaviour was also assessed[16,22]. The results obtained by these authors have clearly shown the effectiveness of these analytical models.

The numerical approach proposed in this work has been tested to simulate the fatigue crack propagation in a friction stir-welded specimen. The residual stress field obtained from the simulation of an elastic–plastic friction stir welding (FSW) process has been adopted as the initial stress scenario for fatigue crack propagation[23]. For the sake of brevity, a complete description of the FSW process has been omitted because it was already well explained in previous works[24-27]. Furthermore, an assessment of the propagation life of the same friction stir weldment has been previously carried out adopting by linear elastic fracture mechanics (LEFM).[24,25]

As the small-scale yielding (SSY) condition is both at the basis of LEFM and at the basis of non-linear fracture mechanics (NLFM), the SSY condition can be also considered as an extension of LEFM[28]. Thus, the energy release rate (ERR) can be considered as equivalent to the stress intensity factor (SIF) because in the SSY, the equation $J = K^2/E$ is still valid.

To avoid confusion in the present contribution, it is worth noting that the crack closure effect has not been produced by PICC along the crack flanks, but only by the compressive state of the residual stress field, coming from an elastic–plastic simulation of a previous FSW process[24-27], which acts on the flanks of a crack. Then, the fatigue crack propagation has been simulated by means of two commercial FE-based software packages (Abaqus and Zencrack) and the modified Kujawski-Ellyin (KE) fatigue propagation law for non-linear problems in SSY conditions. Hence, the fatigue propagation has been carried out similar to an elastic analysis in which the plasticity, developed during the crack propagation along the crack flanks, has not been taken into account. Thus, also other effects like oxide-induced closure and roughness-induced closure have not been considered in the numerical analysis.

However, differently by LEFM approach, in SSY conditions, the material yielding is considered, and thus, taking into account the Irwin theory in which a fictitious crack extension used for estimating the plastic zone size, a_{eff}, and the corresponding effective SIF, K_{eff}, can be obtained[28]. Because the residual stress field is three-dimensional, in the KE non-linear law for fatigue crack propagation, an equivalent range of the SIF, ΔK_{eff}, has been adopted.

Furthermore, the KE model is considered based on the concept of a fracture process zone (FPZ), a small region ahead to the crack front, that is called the "plastic zone," in which the stable growth process is substantially associated with a yielding[15].

2 | MATERIALS AND METHODS

This section describes the approach developed in this paper. As the determination of the *J*-integral, in finite element (FE) codes, is based on the domain integral method in contour integral evaluation, which was initially

suggested by Parks[29,30] and further developed by DeLorenzi,[31,32] and the domain integral is based on the amount of energy applied to a finite region of elements, the effect of stress discontinuities or any other numerical inaccuracy of the local field quantities is less. Furthermore, this method is considerably robust, and precise values can also be obtained using relatively coarse meshes. As the *J*-integral is also defined in terms of ERR associated with a fictitious advancement of small cracks, the domain integral method is also known as the "virtual crack extension" (VCE) method.[28]

To advance the crack, Zencrack[33] works with contour integral evaluation and the VCE method. Thus, to make the fatigue calculation, it is not necessary to apply a cyclic remote load but only a static load up to its maximum value. Furthermore, in constant amplitude loading, the *R*-ratio is used for calculating the minimum SIF and then ΔK. With this approach, the unloading of the specimen never occurs, and the material behaviour is non-linear.

Then, two cracks are introduced in the uncracked FE model by means of the constrained crack faces technique (CCFT)[23,24]. By adopting this technique, such defects cannot be considered as "cracks" because of the enforcement of the material continuity due to the application of contact constraints preventing the interpenetration and mutual displacement of the crack faces. Thus, the "cracked" FE model is equivalent to the uncracked one. A residual stress field is introduced in the FE model and employed as an initial stress condition in the fatigue crack propagation[24]. Before carrying out the simulation related to the fatigue crack propagation, the contact constraints, previously imposed on the crack faces, have to be removed by allowing the residual stresses to be redistributed, thereby leading to a new equilibrium condition[24]. In other words, the contact constraints imposed on the crack faces must first be removed, and then a fatigue load can be applied on one side of the specimen, while some constraints that prevent displacements along the three directions of the global reference system have to be applied on the other side.

To increase the accuracy, the crack growth simulation is divided into two distinct steps. The first spans up to when one of the cracks named "the central crack" becomes through-thick, namely, when only two crack fronts are modelled. The second step initiates starting from the through-thickness crack, namely, when three crack fronts are modelled. The overall fatigue crack propagation spans until the number of cycles provided by the experimental test is matched. Hence, two crack growth simulations are carried out using the KE model considering a non-linear behaviour for the material under the hypothesis of SSY. The material adopted in the present simulations is the AA2024-T3, which is modelled accordingly to Ramberg-Osgood equation (1) and obtained from the true stress–strain curve shown in Figure 1[23].

$$\varepsilon = \frac{\sigma}{E} + 0.002\left(\frac{\sigma}{\sigma_0}\right)^{1/n}, \tag{1}$$

where $n = 0.09116$ is the strain hardening coefficient, $E = 70\,000$ MPa is the Young modulus, and σ_0 is the tensile yielding strength of the material.

2.1 | Geometry, loads, and boundary conditions

The same geometric model adopted to obtain the residual stress field[23] has been used for the numerical fatigue crack propagation (see Figure 2). The fatigue load (24 kN) is applied with a uniform distribution of tractions on the upper surface of the specimen (100 MPa), with an *R*-ratio equal to 0.1 (Figure 2).

Hence, the residual stress field is imported into the model for fatigue crack propagation, while the constraints previously imposed on the crack faces are removed, thereby allowing the cracks to open (Figure 3).

In this way, the residual stresses can be redistributed before the simulation of the crack growth[24]. Furthermore, such a redistribution involves the whole domain. In a following step, the fatigue load is applied on the specimen, and the simulation of the crack growth can initiate. This part of the simulation is driven by the non-linear propagation law introduced in the model. Finally, the simulation of the crack propagation is concluded once the expected number of cycles is reached from the experimental test.

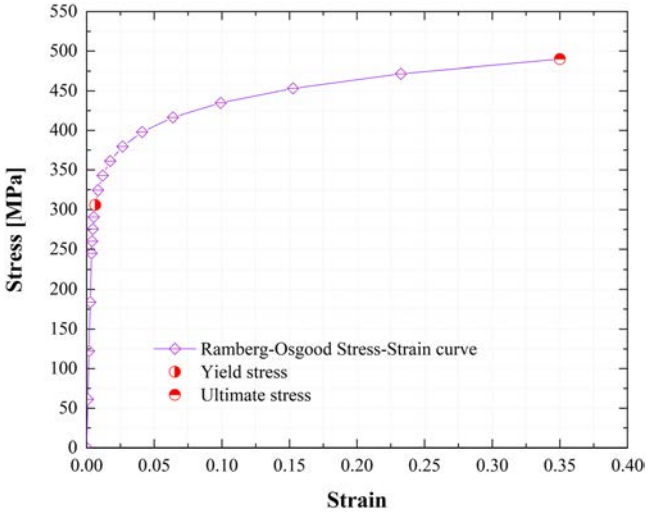

FIGURE 1 Ramberg-Osgood stress–strain curve for AA2024-T3 [Colour figure can be viewed at wileyonlinelibrary.com]

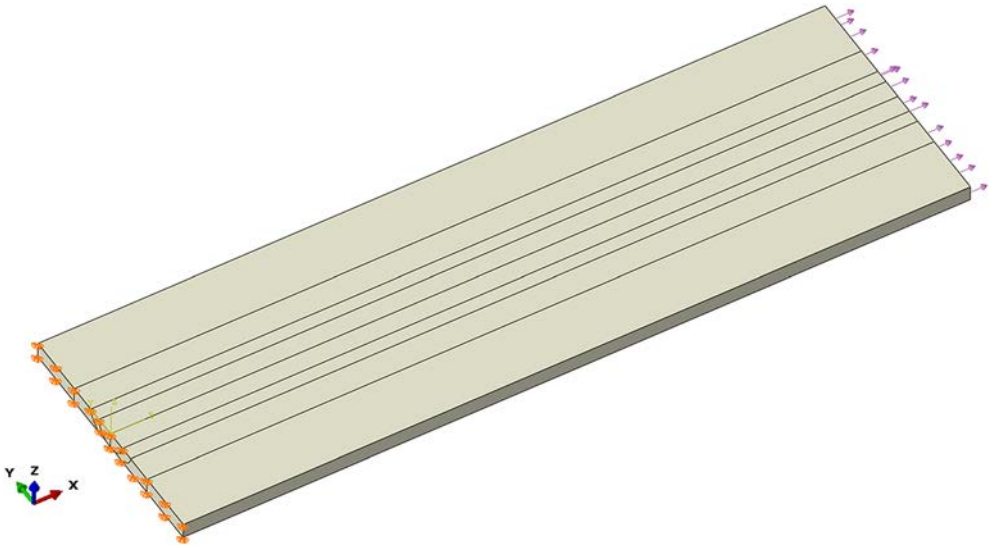

FIGURE 2 Model geometry of the specimen with the boundary and loading conditions highlighted [Colour figure can be viewed at wileyonlinelibrary.com]

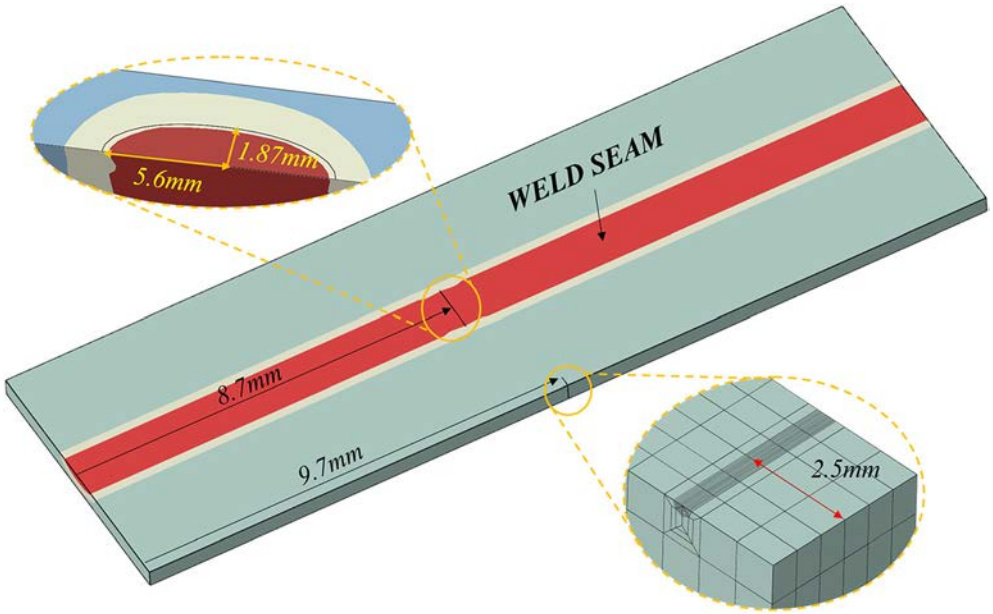

FIGURE 3 Crack positions and dimensions with highlighting of some details of the lateral crack [Colour figure can be viewed at wileyonlinelibrary.com]

Furthermore, it can be observed that when the remote load is applied to the welded joint, a stress state is generated. Such a stress and the residual stress are distributed throughout the domain. The sum of these two stresses represents the overall stress over the component.

3 | NON-LINEAR MODIFIED KE LAW FOR FATIGUE CRACK PROPAGATION

A material obeying the following cyclic stress–strain relationship is considered:

$$\sigma = E\varepsilon \quad \text{for} \quad \sigma < \sigma_0, \tag{1a}$$

$$\sigma = \sigma_0\left({}^{\varepsilon}/_{\varepsilon_0}\right) \quad \text{for} \quad \sigma \geq \sigma_0, \tag{1b}$$

where $\sigma_0 = E\varepsilon_0$ is the tensile yield strength; the maximum cyclic stress and strain components normal to the plane of the crack growth within the monotonic plastic zone (MPZ) can be rewritten as follows:

$$\sigma^m_{max} = \sigma_0\left\{\frac{K^2_{max}}{(1+n')\pi\sigma_0^2 x.}\right\}^{\frac{n'}{(1+n'),}} \tag{2}$$

$$\varepsilon_{max}^{m} = \varepsilon_0 \left\{ \frac{K_{max}^2}{(1+n')\pi\sigma_0^2 x.} \right\}^{\frac{1}{(1+n'),}} \quad (3)$$

where n' is the cyclic hardening exponent and x is the distance from the crack tip. In order to consider the cyclic plastic zone (CPZ), the cyclic yield strength, $\sigma_y^{'}$, needs to be taken into account. Then, the maximum cyclic stress and strain components, which are normal to the plane of the crack growth within the CPZ, can be written as follows:

$$\sigma_{max}^{c} = \sigma_y^{'} \left\{ \frac{K_{max}^2}{(1+n')\pi\sigma_y^{'}\delta^{*}.} \right\}^{\frac{n'}{(1+n'),}} \quad (4)$$

$$\varepsilon_{max}^{c} = \varepsilon_y^{'} \left\{ \frac{K_{max}^2}{(1+n')\pi\sigma_y^{'}\delta^{*}.} \right\}^{\frac{1}{(1+n').}} \quad (5)$$

Similar to x, δ^* is a length in the crack extension direction, called the FPZ, in which the majority of the damage is experienced by the material,[11] while n' and $\sigma_y^{'}$ are the same parameters just described. The MPZ size at the maximum load, r_m, and the CPZ size, r_c, can be expressed as follows:

$$r_m = \frac{1}{(1+n')\pi} \left(\frac{K_{max}}{\sigma_0} \right)^2, \quad (6)$$

$$r_c = \frac{1}{4(1+n')\pi} \left(\frac{\Delta K}{\sigma_y^{'}} \right)^2. \quad (7)$$

In the unmodified version of the KE model, δ^* is written as

$$\delta^* = \frac{\Delta K_{th}^2}{4\pi E\varepsilon_f^{'}(1+n')(\sigma_f^{'} - \sigma_m).}, \quad (8)$$

and this value is set as a constant representing a material length parameter. In this work, another expression of δ^* was used and reported in Equation (9), as proposed by Li et al[17]:

$$\delta^* = \frac{(\Delta K^2 - \Delta K_{th}^2)}{\left(\pi E\sigma_y^{'}\right)}, \quad (9)$$

where δ^* is now a parameter depending on the driving force of the stress–strain field, ΔK.

To account for crack blunting effects, a critical crack blunting radius, ρ_c, is introduced, which is associated with ΔK_{th}. Furthermore, ρ_c can be expressed according to the concept of the crack opening displacement as

$$\rho_c = \frac{\Delta K_{th}^2}{\left(\pi E\sigma_y^{'}\right)}, \quad (10)$$

and the cyclic yield strength, $\sigma_y^{'}$, is described in Equation (11) as proposed by Jing et al[34]:

$$\sigma_y^{'} = (1+\overline{x})^{*}\sigma_u^{*}\left\{ {}^{-}0.002/_{log}(1-\overline{x}). \right\}^{0.16}, \quad (11)$$

where σ_u is the ultimate strength and $\overline{x} = 0.203$ is the reduction in the area (material reference: Boller and Seeger). Then, material and low-cycle fatigue properties are reported in Table 1,[23] where ΔK_{th} is the threshold value of SIF, E is the Young modulus, υ is the Poisson ratio, $\sigma_f^{'}$ is the fatigue strength coefficient, $\varepsilon_f^{'}$ is the fatigue ductility coefficient, and b and c are the fatigue strength exponent and the fatigue ductility exponent, respectively.

Zencrack calculates the ERR after that it makes a conversion to K. The conversion factor (f_{conv}) can be expressed with Equation (12):

$$f_{conv} = \sqrt{E(1-\upsilon^2)} \quad (12)$$

and it is applied to Equation (13) to calculate the SIF factor range, ΔK, as follows:

$$\Delta K = \Delta\sqrt{J}.\ f_{conv}. \quad (13)$$

Finally, the fatigue crack growth (FCG) law for nonlinear materials can be written as follows:

$$\frac{da}{dN} = 2\delta^* \left\{ \frac{\left(\Delta K^2 - \Delta K_{th}^2\right)}{4(1+n')\left(\sigma_f^{'} - \sigma_m\right)\pi E\varepsilon_f^{'}\delta^{*}.} \right\}^{1/\beta}, \quad (14)$$

where $\beta = -(b+c)$ and σ_m is the local mean stress. It is important to underline that the proposed FCG law, shown in Equation (14), is based also on the effect of the local mean stress, which can be written as follows[15]:

$$\sigma_m = \left[\frac{(1+R_s)}{2} \right]^{*}\sigma_{max}, \quad (15)$$

where the stress ratio, R_s, is not generally coincident with the stress ratio, R, which is linked to the remote tensile load, and it depends on the distance from the crack front[15]. Thus, σ_m changes within the plastic zone. In this work and for the sake of brevity, the calculation of the R_s values is referred to the literature.

TABLE 1 Material and LCF parameters (AA2024-T3)

ΔK_{th}, N/mm$^{3/2}$	E, N/mm^2	υ	σ_y', N/mm^2	σ_f', N/mm^2	ϵ_f'	n'	b	c
52	72 000	0.33	320	835	0.174	0.109	−0.096	−0.644

Abbreviation: LCF, low-cycle fatigue.

3.1 | The closure correction

Huffman[35] identified ΔK_{tot} expressed by means of Equation (16) as a ΔK_{eff} in Equation (17). Then, the closure correction is introduced into the KE law by means of Equations (16) and (17).

$$\Delta K_{tot} = \Delta K_{apll}\left\{1 - \left[\frac{(\sigma_{0.05} - \sigma_0)}{\sigma_{0.05}}\right](1 - R)\right\}, \quad (16)$$

$$\Delta K_{eff} = \Delta K_{tot}, \quad (17)$$

where $\sigma_{0.05}$ is the stress value corresponding to $\varepsilon = 0.05$, on the true stress–strain curve shown in Figure 1,[35] and σ_0 is the material yield strength while ΔK_{appl} is the current ΔK obtained from the J-integral conversion by using of Equation (13). Based on these equations, the closure term, U_{cl}, can be expressed as follows:

$$U_{cl} = \frac{\Delta K_{eff}}{\Delta K}. \quad (18)$$

In the previous literature, it has been experimentally shown the effect of the R-ratio in the near-threshold regime and that ΔK_{th} must be corrected to have an effective stress intensity range $\Delta K_{th,eff}$, able to fully consider the crack closure effect. Thus, using Equation (18), the $\Delta K_{th,eff}$ can be derived and expressed as follows:

$$\Delta K_{th,eff} = \Delta K_{th} * U_{cl}. \quad (19)$$

The above equations have been all introduced in the code to obtain automatically the closure parameters during the crack growth in a similar way to the other parameters of fatigue crack propagation. Finally, considering $\Delta K_{th,eff}$ described in Equation (19), Equations (9) and (10) can be rewritten as follows:

$$\delta^* = \frac{\left(\Delta K^2 - \Delta K_{th,eff}^2\right)}{\left(\pi E \sigma_y'\right)} \text{ and} \quad (20)$$

$$\rho_c = \frac{\Delta K_{th,eff}^2}{\left(\pi E \sigma_y'\right)}. \quad (21)$$

Then, the FPZ will be the sum of $\delta^* + \rho_c$ that is reported in Equations (20) and (21).

4 | RESULTS AND DISCUSSION

4.1 | Thermal-stress analysis

The model used for the calculation of the residual stress field and for fatigue crack propagation has the same number of linear elements (111 887, C3D8) with 115 001 nodes. The longitudinal residual stresses have been obtained from an elastic–plastic analysis for the simulation of the FSW process[36,37]. Points A_1, B_1, C_1 and A_2, B_2, C_2 positioned along the fronts of the lateral and central cracks, respectively (Figure 5), are used for measuring the crack's advancement during the propagation. Hence, points C_1 and C_2 are positioned at the middle of the lateral and central crack fronts, respectively, while measuring points A_1, A_2 and B_1, B_2 are related to the intersection of the crack fronts with the free surfaces of the specimen.

In the welded specimen, the equilibrium condition is achieved by combining the stresses in the areas immediately surrounding the weld bead. This peculiarity of the welding process can be clearly distinguished from the observation of the residual stress distribution shown in Figure 4, where the numerical and experimental residual stress profiles are reported in the midline of the thickness, at the end of the releasing step, and for the uncracked model configuration[23,27].

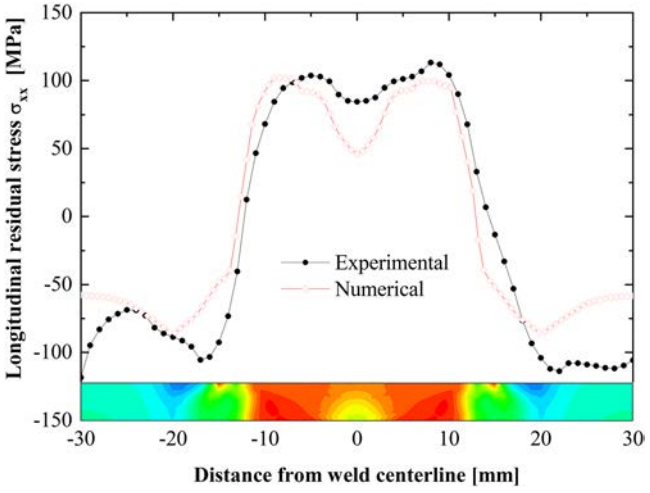

FIGURE 4 Residual stress profiles evaluated on the section containing the central crack [Colour figure can be viewed at wileyonlinelibrary.com]

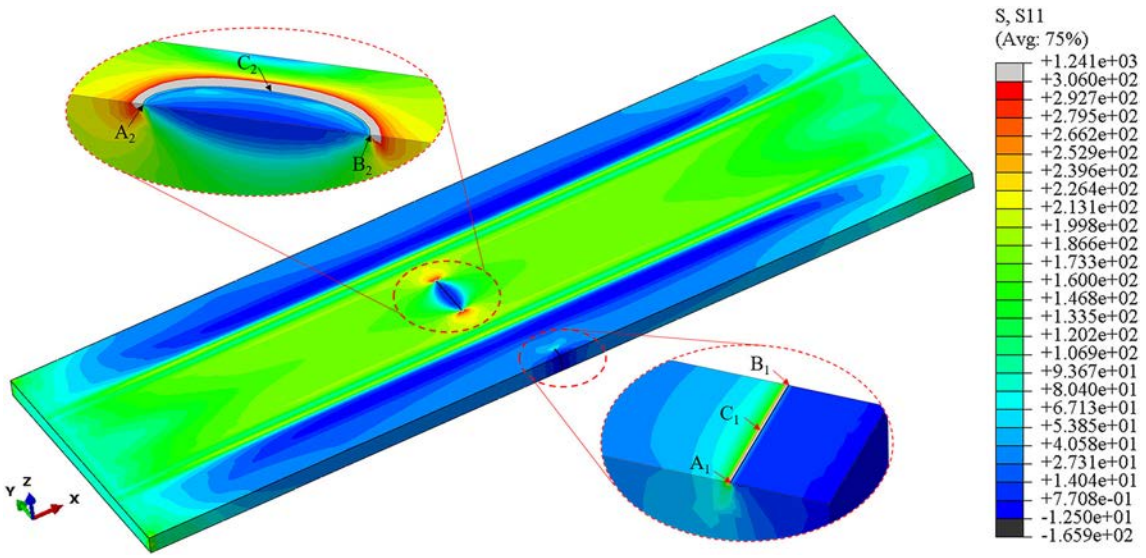

FIGURE 5 Principal stress along the *X*-direction (MPa) with highlighted cracked regions [Colour figure can be viewed at wileyonlinelibrary.com]

It is worth noting that the residual stress field obtained from the elastic–plastic simulation of the FSW process is reported only in the longitudinal direction of the specimen because the corresponding experimental results are calculated by using the contour method[27].

4.2 | The non-linear KE model with closure correction

The crack is modelled in such a way that the root of the crack front can proportionally blunt the applied load. Hence, the use of the VCE allows to carry out the crack insertion through incremental steps. Each step is then divided into two sub-steps. In the first (substep0), the constraints applied on the crack faces are removed, and the redistribution of the residual stresses occurs. In the second (substep1), the fatigue load is applied (Figure 5).

In Figure 6A,B, the crack growth rates for the lateral and central cracks, respectively, are shown. If the closure correction is not applied, the lateral crack does not propagate[24]; ie, all the nodes positioned along the crack front do not exceed the threshold limit ΔK_{th}, and this differs from what happens in the experimental practice. This fact is due to the compressive nature of the residual stress field that prevents the lateral crack from opening. Thus, a closure condition should be taken into account, and then ΔK_{th} should be corrected to have a $\Delta K_{th,eff}$. Furthermore, the value of $\Delta K_{th,eff}$ will be lower than the starting value of ΔK_{th} so as to allow the lateral crack to open and propagate[38].

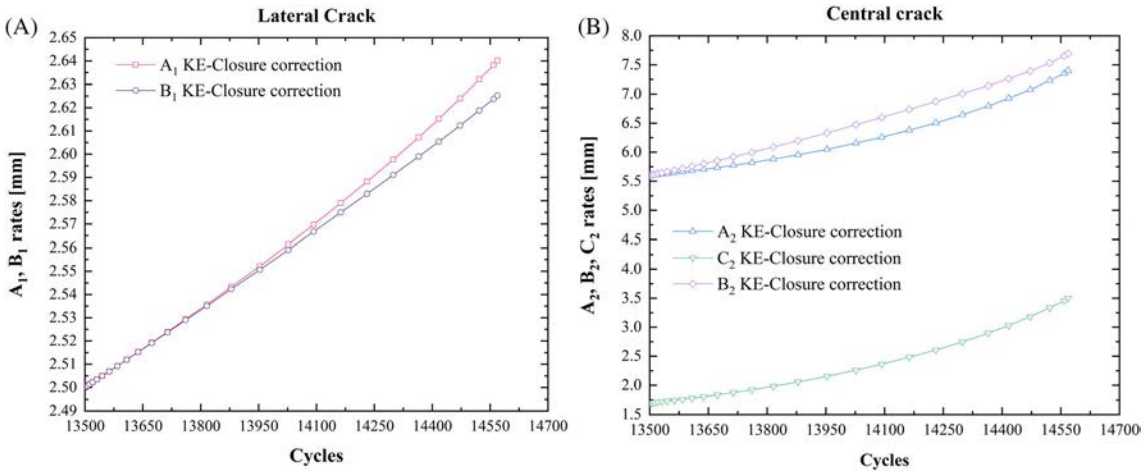

FIGURES 6 Growth rates of (A) points A_1, B_1, A_2, B_2 and (B) C_2 obtained from the lateral and central crack propagations, respectively [Colour figure can be viewed at wileyonlinelibrary.com]

Points A_1, B_1 and A_2, B_2 are related to the intersection between the free surfaces of the specimen and the fronts of the lateral crack (Figure 6A). The central crack depth, by means of the C_2 point, is also shown in Figure 6B.

Hence, two cracks propagate together inside the material. As expected, the central crack grows quicker than the lateral crack, and this behaviour is evident up to when the central crack becomes through-thick. After about 1100 cycles of fatigue propagation, the central crack becomes through-thick, and its front can be divided into two new crack fronts. In Figures 7A,B and 8A,B, some pictures, at various steps of the central and lateral crack fatigue propagation, are shown respectively.

In Figure 9, the growth rates for point A_1 of the lateral crack are shown. In this case, the overall rates of point A_1 are reported, namely, the rates related to the fatigue propagation with two and three crack fronts, respectively, by using the technique explained in the works of Lepore et al[23,24] and Maligno et al.[39] As previously stated, A_1 is a point obtained by the intersection of the lateral crack front with the free surface of the welded sample.

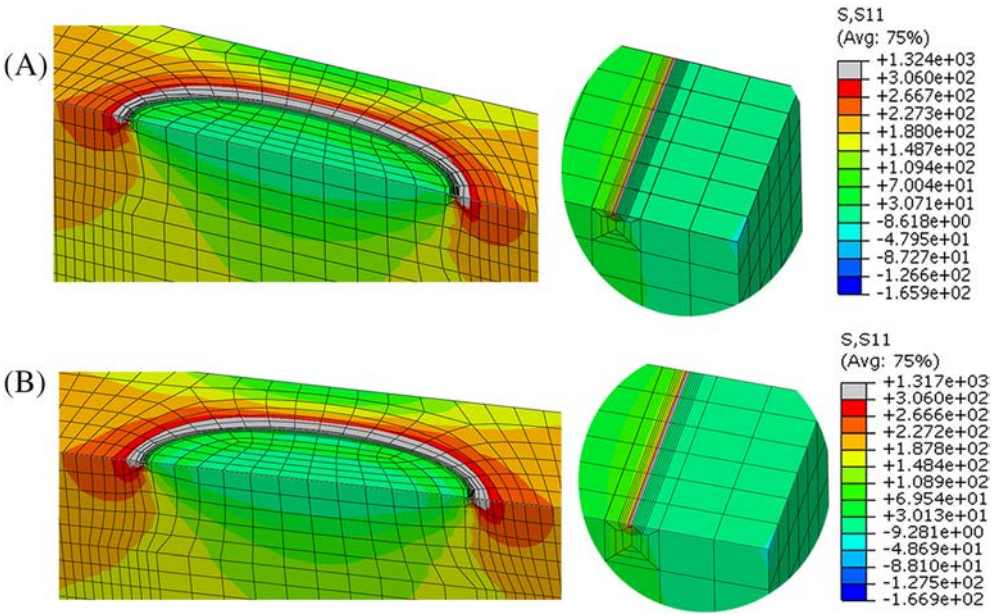

FIGURES 7 A and B, Principal stress distribution (MPa) in the cracked regions (*X*-direction) [Colour figure can be viewed at wileyonlinelibrary.com]

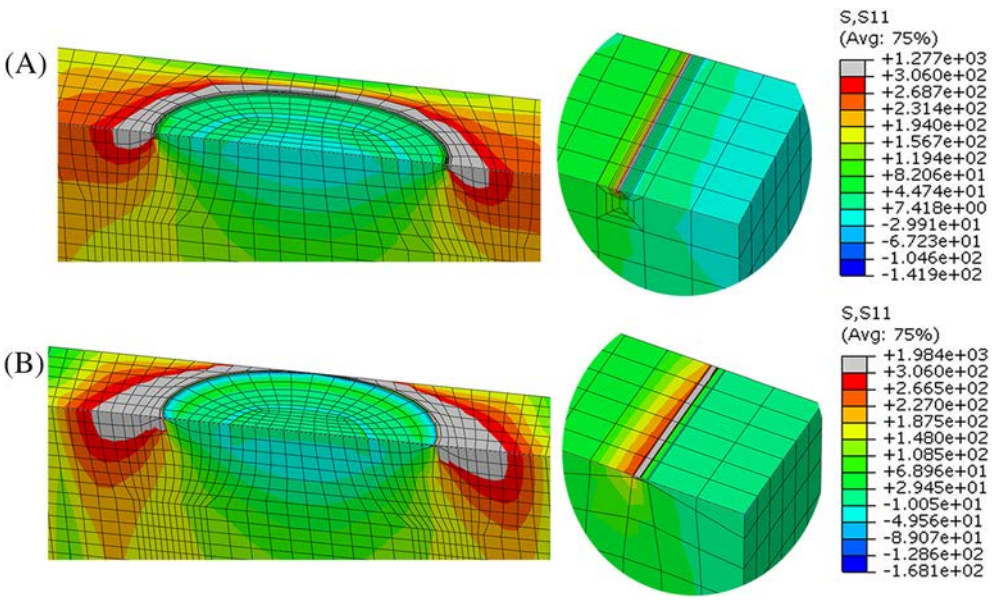

FIGURES 8 A and B, Principal stress distribution (MPa) in the cracked regions (*X*-direction) [Colour figure can be viewed at wileyonlinelibrary.com]

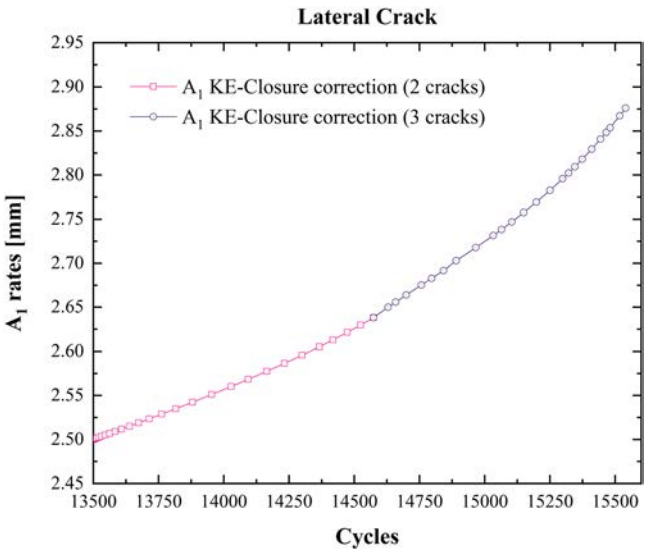

FIGURE 9 Growth rates of point A_1 for the overall propagation of the lateral crack with two and three crack fronts, respectively. KE, Kujawski-Ellyin [Colour figure can be viewed at wileyonlinelibrary.com]

Figure 10A,B shows the principal stress distribution (*X*-direction of the global reference system) for the lateral crack. Initially, both the lateral and central crack fronts are modelled as sharp. However, a line of supplementary nodes has been employed in the model given the possibility that the crack root is proportionally blunt with application of the remote load[27]. Here, it is interesting to observe a moderate blunting of the lateral crack front. The upper bound of the scale is the yield strength (306 MPa) of the adopted alloy AA2024-T3.

Abaqus[40] and Zencrack interact in each other in such a way that fatigue propagation of the crack is obtained by means of a series of incremental steps in which the maximum value of the applied remote load is reached. Then, the number of cycles is calculated by means of the fatigue law introduced in Zencrack with an external FORTRAN routine. Figure 11 shows the MPZ in a polar diagram obtained from the FEM-based analysis at the crack insertion. The dimensions of the MPZ are clearly highlighted within the polar diagram, in which the extension of that zone is plotted as a periodic function.

4.2.1 | An assessment of plastic zones

In this section, a comparison among the FPZ, CPZ, and MPZ that are related to the KE model with and without the closure correction, for the case with two cracks, is shown for the lateral and central cracks, respectively. These quantities are calculated by means of the external routine with analytical equations reported in Section 3. As there are oscillations of these values calculated along the crack fronts then, in Figures 12, 13, and 14, all the

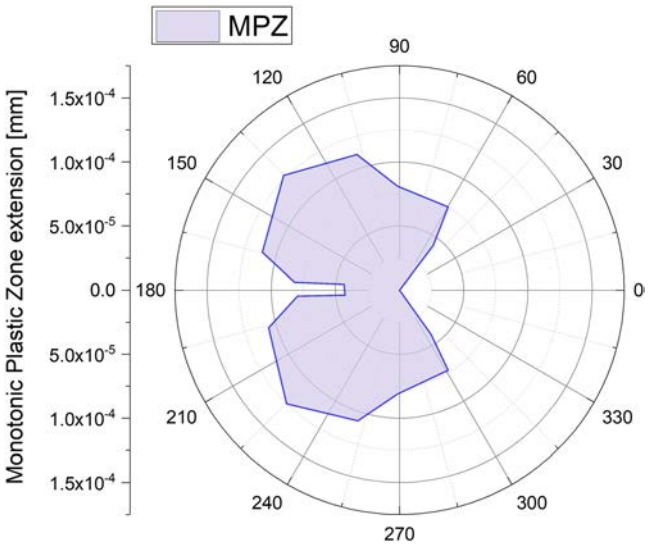

FIGURE 11 Polar diagram of the monotonic plastic zone (MPZ) in the near tip field for the lateral crack (first step with three cracks) [Colour figure can be viewed at wileyonlinelibrary.com]

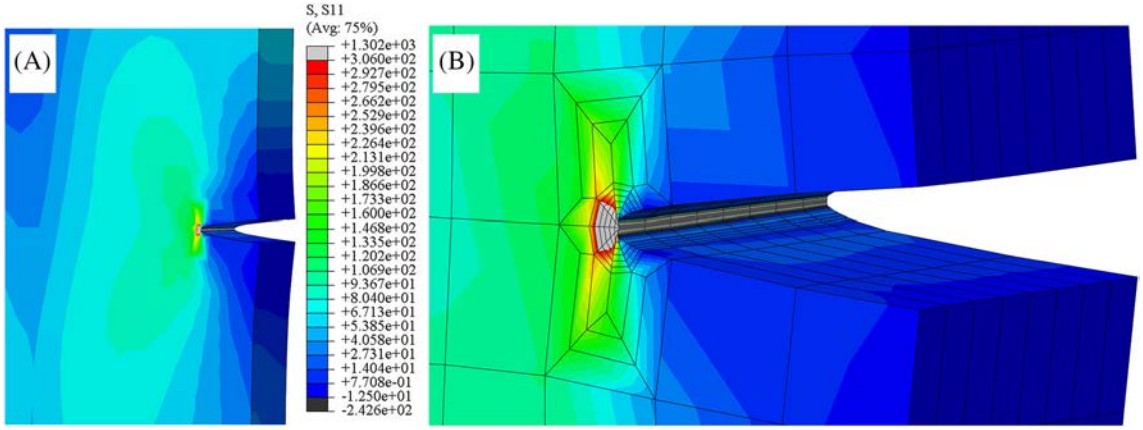

FIGURES 10 Principal stress distribution (MPa) along the *X*-direction for the lateral crack (A) with highlighting of the lateral crack zoom (B) and related to the first step of fatigue crack growth with three crack fronts [Colour figure can be viewed at wileyonlinelibrary.com]

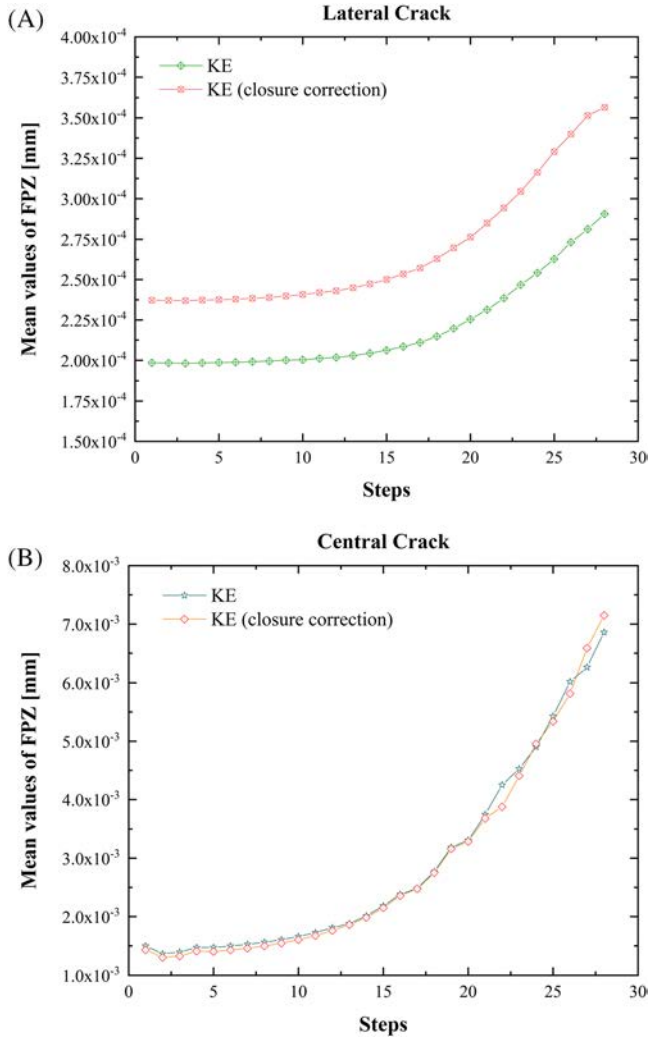

FIGURE 12 A, Mean values of the fracture process zones (FPZs) for the lateral crack. B, Mean values of the FPZs for the central crack. KE, Kujawski-Ellyin [Colour figure can be viewed at wileyonlinelibrary.com]

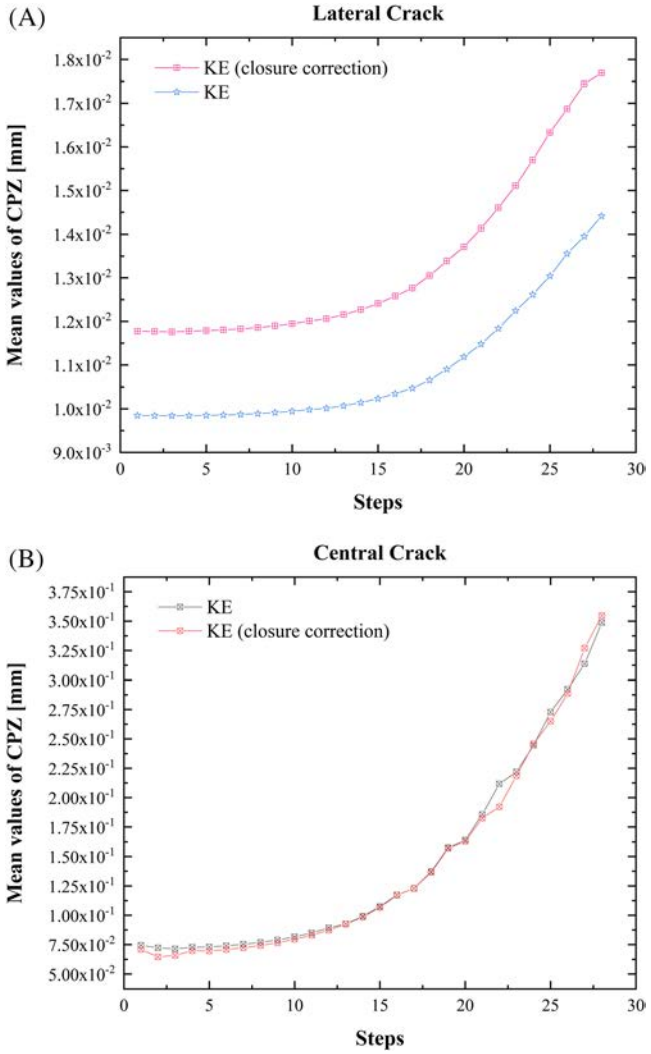

FIGURE 13 A, Mean values of the cyclic process zone (CPZ) for the lateral crack. B, Mean values of the CPZ for the central crack. KE, Kujawski-Ellyin [Colour figure can be viewed at wileyonlinelibrary.com]

values of process zones are reported as the mean values along the fronts, and for each step of the crack propagation. It is worth noting that the reported values of the FPZ are the sum of $\rho^* + \rho_c$, ie, the lengths of the FPZ and the crack blunting radius at $\theta = 0$. Furthermore, the term for the closure correction, U_{cl}, and calculated at the first step of fatigue crack propagation is equal to 0.87 and 0.48 for the central and lateral cracks, respectively.

In Figure 12A,B, the mean values of the FPZ for each step of the grown crack are reported. These values of the FPZ, which are obtained considering the KE model with closure correction, are higher than the respective values obtained without closure correction. This result is consistent with Equation (20) and the results reported by Blom et al.[38] Then, as expected, for each node of the crack fronts, the length of the blunt crack has a constant value during all the fatigue crack propagations, using the model either with or without closure correction. These values are equal to 3.66E−5 mm for the KE model without closure correction and 1.23E−5 mm for the model with closure correction.

In Figure 13A,B, the mean values of the CPZs for the lateral crack are shown. As expected, the use of $\Delta K_{th,eff}$ produces an increase effect on the CPZ length of the lateral crack where the compressive residual stresses act, while it is expected that the length of the plastic zone does not change for the central crack where the residual stresses are traction (Figure 13B).

In Figure 14A,B, the comparison between the MPZs confirms that closure phenomenon produces an increase of the plastic zone length for the lateral crack, while for the central crack, the length of the MPZ does not changes with the growing crack. It is worth noting that because of

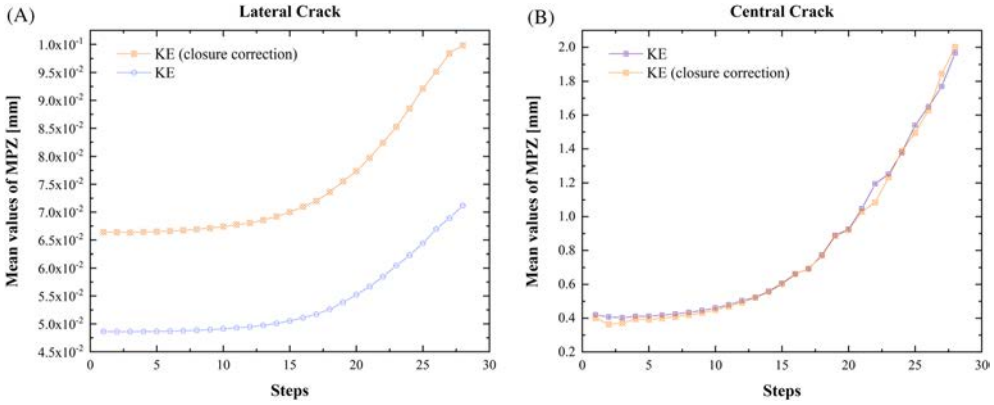

FIGURES 14 Mean values of the monotonic process zone (MPZ): A, for the lateral crack; B, for the central crack. KE, Kujawski-Ellyin [Colour figure can be viewed at wileyonlinelibrary.com]

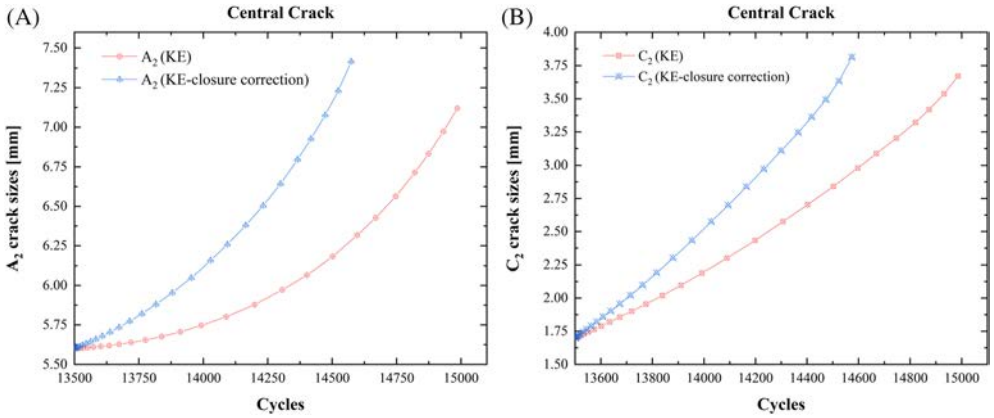

FIGURE 15 Comparison between the A_2 (A) and C_2 (B) growth rates related to the central crack for the Kujawski-Ellyin (KE) model with and without closure correction [Colour figure can be viewed at wileyonlinelibrary.com]

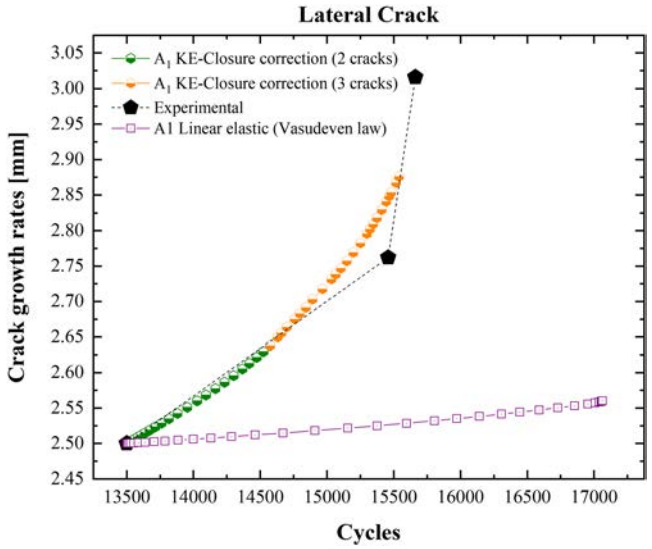

FIGURE 16 Comparison between the numerical and experimental growth rates for the lateral crack propagation before (green) and after (orange) the central crack becomes through-thick. KE, Kujawski-Ellyin [Colour figure can be viewed at wileyonlinelibrary.com]

the FORTRAN routines introduced in Zencrack for the KE model with closure correction, the $\Delta K_{th,eff}$ is applied to the propagation of either the lateral or central crack. However, the same happens when ΔK_{th} is applied to the KE model without closure correction.

5 | CRACK GROWTH RATE COMPARISON

In Figure 15A,B, the comparison between the growth rates for points A_2 and C_2 (see Figure 5) of the central crack is shown. In this case, a satisfactory agreement between the numerical data related to the KE model without the closure correction cannot be found. The KE model with closure correction shows an increase of the growth rates because the length of the FPZ is greater than what is obtained without considering closure correction. Then, a larger FPZ results in greater damage, thus resulting in fewer cycles to arrive at the estimated end point of fatigue crack propagation.

In Figure 16, the comparison between the numerical and experimental results for the lateral crack is highlighted. Three experimental points were obtained during the experimental test[26,27] by means of two crack gauges located near the lateral crack front[26,27]. Thus, Figure 16 is related to a condition of the sample in which the lateral crack has propagated by 2.50 mm. This condition corresponds to the beginning of the central crack propagation. Then, the graph shown in Figure 16 refers to the lateral crack propagation before and after the central crack becomes through-thick by using the KE model with closure correction. Such a model is adopted for growing two and three crack fronts, respectively. By observing Figure 16, it is noted that a good agreement between the numerical and experimental results can be found. For the sake of completeness, Figure 16 also shows the growth rates of the point related to the linear analysis[24].

6 | CONCLUSIONS

In this work, the residual stress field obtained by the numerical simulation of an FSW process has been employed as the starting condition to assess the fatigue propagation of three-dimensional cracks in a friction stir-welded component. All the simulations have been carried out by using FEM-based commercial software. The non-linear material behaviour has been modelled by means of the Ramberg-Osgood equation. Hence, the KE non-linear model for fatigue crack propagation has been taken into account in SSY conditions. Furthermore, the crack fronts have been modelled to consider the blunting effect. Then, two different fatigue crack propagation simulations have been carried out based on the KE law with and without closure correction. Initially, only two cracks have been introduced in the welded sample, while at the end of the fatigue crack propagation, three overall cracks have been considered in the welded component. Furthermore, an assessment of the plastic zone extension for the KE model with and without the closure correction has been performed, and a comparison between the experimental and numerical crack growth rates of the lateral crack has been carried out, showing a satisfactory agreement.

The main conclusions produced by this study can be summarized as follows:

- A residual stress field coming from the simulation of a FSW process has been assumed as an initial stress condition.
- The KE model for the fatigue crack propagation has been implemented in the numerical FEM-based analysis by assuming non-linear material behaviour with and without crack closure correction.
- The assessment of the extension of FPZ and cyclic and MPZs has been carried out by using the KE model with and without crack closure correction, respectively.
- A satisfactory agreement between the numerical and experimental crack growth rates for the lateral crack has been found.

REFERENCES

1. Pippan R, Hohenwarter A. Fatigue crack closure: a review of the physical phenomena. *Fatigue Fract Eng Mater Struct*. 2017;40(4): 471-495.
2. Ferro P, Berto F, James NM. Asymptotic residual stress distribution induced by multipass welding processes. *International Journal of Fatigue*. 2017;101:421-429.
3. Ferro P, Berto F, James NM. A simplified model for TIG-dressing numerical simulation. *Model Simul Mater Sci Eng*. 2017;25(3):035012.
4. Ferro P, Berto F, James NM. Asymptotic residual stresses in butt-welded joints under fatigue loading. *Theor Appl Fract Mech*. 2016;83:114-124.
5. Ferro P, Berto F. Quantification of the influence of residual stresses on fatigue strength of Al-alloy welded joints by means of the local strain energy density approach. *Strength of Materials*. 2016;48:426-436.
6. Ritchie RO. Mechanisms of fatigue crack propagation in metals, ceramics and composites: role of crack tip shielding. *Mater Sci Eng A*. 1988;103:15-28.
7. Suresh S. *Fatigue of Materials*. Cambridge: Cambridge University Press; 1991.
8. Elber W. The significance of fatigue crack closure. *ASTM international*. 1971. STP 486 Damage tolerance in aircraft structures;230-242.
9. Elber W. Fatigue crack closure under cyclic tension. *Eng Fract Mech*. 1970;2:37-45.
10. McEvily AJ. On crack closure in fatigue crack growth. *ASTM International*. 1988. STP 982 Mechanics of Fatigue Crack Closure;35-43.
11. Louat N, Sadananda K, Duesbery M, Vasudevan AK. A theoretical evaluation of crack closure. *Metall Trans A*. 1993;24(10): 2225-2232.
12. Vasudeven AK, Sadananda K, Louat N. A review of crack closure, fatigue crack threshold and related phenomena. *Mater Sci Eng A*. 1994;188(1-2):1-22.

13. Huffman PJ. A strain energy based damage model for fatigue crack initiation and growth. *International Journal of Fatigue*. 2016;88:197-204.
14. Shi KK, Cai LX, Chen L, Wu SC, Bao C. Prediction of fatigue crack growth based on low cycle fatigue properties. *Int J Fatigue*. 2014;61:220-225.
15. Kujawski D, Ellyin F. A fatigue crack growth model with load ratio effects. *Eng Fract Mech*. 1987;28(4):367-378.
16. Kujawski D, Ellyin F. On the size of plastic zone ahead of crack tip. *Eng Fract Mech*. 1986;25(2):229-236.
17. Li DM, Nam WJ, Lee CS. An improvement on prediction of fatigue crack growth from low cycle fatigue properties. *Eng Fract Mech*. 1998;60(4):397-406.
18. Noroozi AH, Glinka G, Lambert S. A two parameter driving force for fatigue crack growth analysis. *Int J Fatigue*. 2005; 27(10-12):1277-1296.
19. Song XX, Shang YB, Shi HJ, Niu LS, Wang ZX. Plastic mismatch effect on plasticity induced crack closure: fatigue crack propagation perpendicularly across a plastically mismatched interface. *Fatigue Fract Eng Mater Struct*. 2019;42:597-611.
20. Tong J, Alshammrei S, Wigger T, Lupton C, Yates JR. Full-field characterization of a fatigue crack: crack closure revisited. *Fatigue Fract Eng Mater Struct*. 2018;41:2130-2139.
21. Akhtar N, Wu SJ. Macromechanics study of stable fatigue crack growth in Al-Cu-Li-Mg-Ag alloy. *Fatigue Fract Eng Mater Struct*. 2017;40:233-244.
22. Noroozi AH, Glinka G, Lambert S. A study of the stress ratio effects on fatigue crack growth using the unified two-parameter fatigue crack growth driving force. *Int J Fatigue*. 2007;29(9-11): 1616-1633.
23. Lepore M, Berto F. On the fatigue propagation of multiple cracks in friction stir weldments using linear and non-linear models under cyclic tensile loading. *Eng Fract Mech*. 2019;206:463-484.
24. Lepore M, Carlone P, Berto F, Sonne Mads R. A FEM based methodology to simulate multiple crack propagation in friction stir welds. *Eng Fract Mech*. 2017;184:154-167.
25. Citarella R, Carlone P, Lepore M, Palazzo GS. Numerical-experimental crack growth analysis in AA2024-T3 FSWed butt joints. *Adv Eng Softw*. 2015;80:47-57.
26. Citarella R, Carlone P, Lepore M, Sepe R. Hybrid technique to assess the fatigue performance of multiple cracked FSW joints. *Eng Fract Mech*. 2016;162:38-50.
27. Carlone P, Citarella R, Sonne MR, Hattel JH. Multiple crack growth prediction in AA2024-T3 friction stir welded joints, including manufacturing effects. *International Journal of Fatigue*. 2016;90:69-77.
28. Plasticity BW. *Fracture. Solid Mechanics and Its Applications. 244. Berlin*. Germany: Springer; 2018.
29. Parks DM. A stiffness derivative finite element technique for determination of crack tip stress intensity factors. *Int J Fract*. 1974;10(4):487-502.
30. Parks DM. The virtual crack extension method for non-linear material behaviour. *Comput Methods Appl Mech Eng*. 1977;1: 353-364.
31. DeLorenzi H.G. Energy release rate calculations by the finite element method. General Electric Technical Information Series, Report No. 82CRD205, 1982.
32. DeLorenzi HG. On the energy release rate and the J-integral for 3D crack configurations. *J Fracture*. 1982;19(3):183-193.
33. Zencrack v8.3.1-12,2018. Documentation. Zentech International Limited, 2018.
34. Li J, Sun Q, Zhang Z-p, Li C-w, Qiao Y-j. Theoretical estimation to the cyclic yield strength and fatigue limit for alloy steels. *Mechanics Research Communications*. 2009;36(3):316-321.
35. Huffman PJ. A quantitatively accurate theory of stable crack growth in single phase ductile metal alloys under the influence of cyclic loading. *Graduate Theses and Dissertations*. 2014; 13737.
36. Sonne MR, Tutum CC, Hattel JH, Simar A, de Meester B. The effect of hardening laws and thermal softening on modeling residual stresses in FSW of aluminum alloy 2024-T3. *J Mater Process Technol*. 2013;213:477-486.
37. Sonne MR, Carlone P, Palazzo GS, Hattel JH. Numerical modeling of AA2024-T3 friction stir welding process for residual stress evaluation, including softening effects. *Key Eng Mater*. 2014; 611–612:1675-1682.
38. Blom AF, Holm DK. An experimental and numerical study of crack closure. *Eng Fract Mech*. 1985;22:997-1011.
39. Maligno AR, Rajaratnam S, Leen SB, Williams EJ. A three-dimensional (3D) numerical study of fatigue crack growth using remeshing techniques. *Eng Fract Mech*. 2010;77:94-111.
40. Systems D, Corp S. *Abaqus Analysis User's Manual, Version 6.12.1*. RI, USA: Providence; 2011.